Aerosol and Air Quality Research

Special Issue:
2022 Asian Aerosol Conference (AAC 2022) (II)

REVIEW
https://doi.org/10.4209/aaqr.220343

Face Masks and Prevention of Respiratory Viral Infections: An Overview

Chiu-Sen Wang*

Department of Public Health, National Taiwan University, Taipei 10055, Taiwan

ABSTRACT

Airborne transmission of respiratory viruses consists of three sequential steps: (1) release of respiratory fluids in the form of droplets from the nose and mouth of an infected person, (2) transport of the droplets through air, and (3) entry of the droplets into the nose and mouth of an uninfected individual. Talking, coughing, and sneezing emit droplets across a spectrum of sizes. The water in exhaled droplets begins to evaporate in air and, as a result, the droplets are reduced in size shortly after being emitted. Face masks are effective for capturing droplets just released from the nose and mouth. Studies indicate that more than 50% of community transmission of SARS-CoV-2 is from asymptomatic and pre-symptomatic cases. Use of face masks by the public can effectively reduce the chance of infected individuals unknowingly spreading the virus. In addition to being an effective device for source control, face masks can protect the wearers from inhaling virus-laden droplets. Cloth masks and disposable masks provide reasonable protection for the public, while surgical masks and N95 respirators give higher levels of protection as needed in healthcare settings. Made with varied materials, these masks have different structural characteristics. The collection efficiency of a face mask depends on droplet size, face velocity, and the structural characteristics of the mask. For a given mask, capturing droplets is more effective during exhalation than during inhalation. Pressure drop across the mask should be taken into consideration when selecting a face mask. The best face mask is the one that gives the highest collection efficiency with the least pressure drop. For an effective protection, a mask should fit the face properly. While face masks have proven adequate in reducing airborne transmission of SARS-CoV-2 infections, continuous improvement is needed to better prepare for future respiratory viral threats.

Keywords: Respiratory droplets, SARS-CoV-2, Face masks, Mask efficiency, Fit factor

OPEN ACCESS

Received: October 4, 2022
Revised: October 4, 2022
Accepted: December 12, 2022

* **Corresponding Author:**
cswang@ntu.edu.tw

Publisher:
Taiwan Association for Aerosol Research
ISSN: 1680-8584 print
ISSN: 2071-1409 online

1 INTRODUCTION

SARS-CoV-2, the cause of COVID-19, is a member of the coronavirus family. These viruses use their outer spike protein to attach to the surface of respiratory cells. An infection takes place when the viruses enter the host cells and start to replicate. Respiratory droplets emitted from infected individuals serve as carriers for the viruses to spread to other people. Such airborne transmission has been identified as the primary route for the spread of SARS-CoV-2.

Droplets are produced from respiratory tract lining fluids by expiratory activities such as breathing, coughing, and speaking. Emitted from the mouth and nose, these droplets quickly mix with ambient air. About one half of the water in exhaled droplets evaporates rapidly in ambient air, which has a relative humidity lower than in the respiratory tract. Gravitational settling and convective air currents influence the length of time these droplets remain in air. When the virus-laden droplets move into the breathing zone of an uninfected individual, the receiver's respiratory tract acts as a droplet and virion collector.

Respiratory droplets are aerosol particles. The field of aerosol science deals with the physical and chemical principles that underlie the properties and behavior of particles suspended in air. Application of aerosol science can provide better understanding of respiratory droplets and face

masks that are employed to capture the droplets. Several comprehensive reviews on airborne transmission of respiratory viral infections have appeared over the past two decades (Nicas *et al.*, 2005; Stadnytskyi *et al.*, 2021; Wang *et al.*, 2021). This overview focuses on the aerosol aspects of respiratory virus transmission and how face masks work as devices for source control and personal protection.

2 RESPIRATORY DROPLETS AND VIRIONS

The human respiratory tract consists of three regions: the upper airway region, the tracheobronchial region, and the alveolar region (Fig. 1). The upper airway includes the nasal and oral cavities, the pharynx, and the larynx. The tracheobronchial region covers the airway tree between the trachea and terminal bronchioles. The respiratory bronchioles, alveolar ducts, alveolar sacs, and alveoli make up the alveolar region. From the trachea to the alveoli, the airways bifurcate repeatedly to form a tree-like system consisting on average of 23 generations of branches. The structure of the airways varies markedly from region to region. The trachea and main bronchi have U-shaped cartilage rings in the walls, while the smaller bronchi have irregularly shaped cartilage plates. Unlike the bronchi, the bronchioles have no cartilage. The smooth muscle layer around the bronchioles constricts and dilates to regulate the flow of air.

The respiratory tract epithelial cells are covered with a heterogeneous group of fluids, which differ in chemical composition from region to region. The mucus, an aqueous solution consisting of approximately 95% water, constitutes the top layer of the epithelial fluids. The major solutes in the mucus include sodium ion, potassium ion, chloride ion, lactate, and glycoprotein. Also contained in the respiratory tract lining fluids of an infected person are a large number of virions. For example, the mean SARS-CoV-2 RNA load was about 7×10^6 copies mL^{-1} in the sputum of nine hospitalized COVID-19 patients with no notable disease besides COVID-19 (Wölfel *et al.*, 2020).

2.1 Generation of Respiratory Droplets

Droplets are produced from respiratory tract lining fluids by expiratory activities such as breathing, coughing, sneezing, speaking, singing, and shouting. It is interesting to note that these airborne droplets are human body generated aerosols. In contrast to droplets made with instruments such as a nebulizer, respiratory droplets are aerosols formed from human body fluids through expiratory activities.

The disintegration of liquids, such as breakup of a liquid filament and bursting of a liquid film, is a principal method of aerosol generation. Stadnytskyi *et al.* (2021) summarized the mechanisms

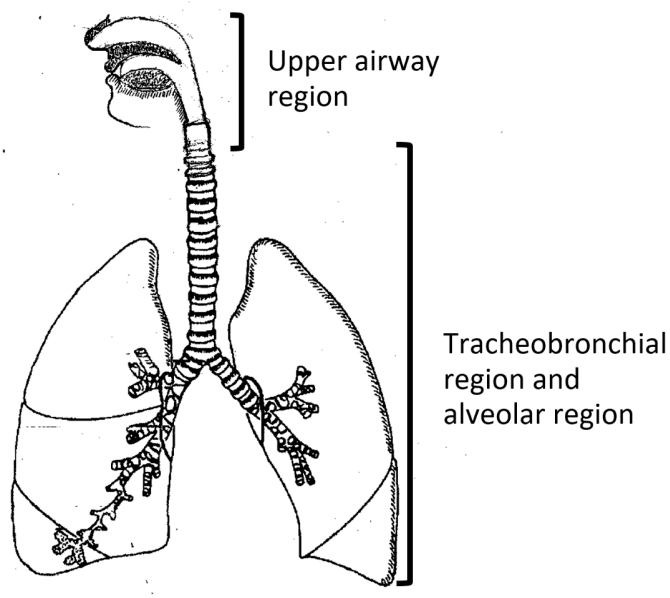

Fig. 1. The human respiratory tract. Adapted from Wang (2005).

of respiratory droplet formation in a recent review on airborne transmission of SARS-CoV-2. During vocalization, large droplets are produced in the oral cavity and smaller droplets formed at the vocal folds. Fluid filaments and films, created when two wetted surfaces separate in the oral cavity and at the vocal folds, become thinner as the surface separation increases. Droplets are generated when the filaments and films are ruptured by exhaled airflow.

Small droplets, 0.01 to 2 μm in diameter, are produced in the alveolar region where the airways close and open during normal breathing. These small droplets are drawn into the alveoli during inhalation and breathed out during exhalation. Coughing, sneezing, and shouting cause rapid airflow, generating droplets of varying sizes in the tracheobronchial region.

During rapid exhalation, the air flow in the upper airways, the trachea, and bronchial tubes becomes turbulent, which causes wave formation in the mucosal layer of these airways. Vocal fold vibration also gives rise to wave formation. Droplets are produced from the waves through wavetop shearing off and film bursting.

2.2 Evaporation of Water from Exhaled Droplets

When droplets are breathed out, the exhaled air blends into the ambient air quickly. Water in the exhaled droplets begins to evaporate because the relative humidity is lower in the ambient air than in the respiratory tract. In addition to the ambient relative humidity, the factors that affect the rate of water evaporation include the droplet diameter, the chemical composition of the droplets, and the ambient temperature. Because there are solutes in the droplet, some water will remain in the droplet if the ambient relative humidity is above the crystallization relative humidity. As a consequence, water will stop evaporating when the droplet reaches the equilibrium diameter, at which there is no net change in the droplet water content.

Using the data on mucus composition reported by Effros *et al.* (2002), Nicas *et al.* (2005) assumed a value of 88 g L^{-1} for the total mass concentration of the nonvolatile species in mucus. Their calculations show that the equilibrium diameter of a mucus droplet is about 0.47 of the initial diameter at 30% relative humidity, and about 0.61 of the initial diameter at 70% relative humidity. Based on these results, one half of the initial diameter has been suggested as a rough estimate of the equilibrium diameter of a respiratory droplet.

The time for a respiratory droplet to attain the equilibrium diameter depends mainly on the initial droplet size and ambient relative humidity. Theoretical calculations show that a droplet, 20 μm in diameter when it is just emitted, will reach the equilibrium diameter in 0.17 s at 30% relative humidity and in 0.4 s at 70% relative humidity (Nicas *et al.*, 2005). Smaller droplets will attain their equilibrium diameters in even shorter time.

Droplets and droplet nuclei have been employed to differentiate the droplets larger than 5 μm in diameter from the smaller particles formed as a result of water evaporation. The reason for using these two terms was that the 5-μm droplet was mistakenly thought to fall rapidly to the ground. In fact, the gravitational settling velocity increases gradually with particle size. A 5-μm droplet falls only 0.0776 centimeters in one second. Both droplets and droplet nuclei are aerosol particles. It is incorrect to separate them into two different groups.

2.3 Exhaled Droplet Size Distributions

Morawska *et al.* (2009) constructed an expiratory droplet investigation system (EDIS) to study the size distribution and sites of origin of exhaled droplets. The system worked as a small wind tunnel into which a volunteer placed his or her head. Filtered air was propelled past the volunteer at a very low velocity. The airflow carried the droplets exhaled by the volunteer to the instrument sampling inlet, which was positioned at a distance downwind. Droplets in the size range of 0.5 to 20 μm were measured using an aerodynamic particle sizer (APS). The results obtained with 15 healthy young volunteers showed that most droplets produced during seven different expiratory activities, including normal breathing and coughing, were in one or more size distribution modes at diameters smaller than 0.8 μm, and a smaller number of droplets were in the mode at 1.8 μm. Speech produced additional droplets in modes near 3.5 and 5 μm, which became more pronounced during sustained vocalization, suggesting that these droplets were mostly generated at the vocal folds. Using these results, Morawska *et al.* (2009) proposed a four-mode model of exhaled droplet size distribution. The equilibrium hygroscopic growth modality of the droplets was found to be

preserved throughout a measurement, indicating that the exhaled droplets reached the equilibrium sizes within 8 s, the time taken for a droplet to travel from a volunteer's nose or mouth to the APS sizing region.

In a subsequent study, Johnson *et al.* (2011) employed the same EDIS to measure the exhaled droplet size distribution over a wider size range. To measure droplets larger than 20 μm, glass slides were placed on the lower inner surface of a section of the sampling duct to catch the settling droplets, and the stain size on glass slides was used to estimate the droplet diameter. Using data collected from 15 healthy young adults, Johnson *et al.* (2011) developed the BLO model for the exhaled droplet size distribution. The model is a tri-modal lognormal distribution. The Bronchiolar Fluid Film Burst mode, "B", contains droplets generated during normal breathing; the Laryngeal mode, "L", includes droplets formed during voicing and coughing; and the Oral Cavity mode, "O", comprises droplets produced during speech and coughing. The number size distributions of droplets calculated from the BLO model show that the count median diameters (prior to evaporative water loss) associated with the three modes are 1.6 μm (B mode), 2.5 μm (L mode), and 145 μm (O mode) for speaking; and 1.6 μm (B mode), 1.7 μm (L mode), and 123 μm (O mode) for coughing. The calculated number concentrations of droplets associated with the three modes are 0.069 cm^{-3} (B mode), 0.085 cm^{-3} (L mode), and 0.001 cm^{-3} (O mode) for speaking; and 0.087 cm^{-3} (B mode), 0.12 cm^{-3} (L mode), and 0.016 cm^{-3} (O mode) for coughing.

Asadi *et al.* (2019) used a HEPA filtered laminar flow hood to investigate the rate of droplet emission during normal speech. Volunteers sat at the hood and spoke into a funnel that was connected to an aerodynamic particle sizer by a conductive silicon tube. Data collected from 48 healthy adults showed that the geometric mean equilibrium diameters of exhaled droplets were approximately 1 μm and the droplet size distribution was independent of the loudness of vocalization. The rate of droplet emission during normal speech increased from approximately 1 to 50 droplets per second as the loudness increased from low to high. A small fraction of volunteers emitted an order of magnitude more droplets than the majority did, suggesting that these superemitters contributed to superspreading of respiratory viral infections.

2.4 Virus-Laden Droplets

The number of SARS-CoV-2 virions an infected individual carries during peak infection is 10^9 to 10^{11}, and a predominant number of the virions are in the lungs (Sender *et al.*, 2021). Thus, droplets generated from the respiratory fluids of a COVID-19 patient very likely carry viruses. For droplets of a given size, the average number of viruses contained in a droplet is proportional to the droplet volume. However, the droplets of the same size do not contain the same number of viruses because the viruses are randomly distributed in the respiratory fluid from which the droplets are generated.

The droplets generated from respiratory fluids are distributed with respect to the droplet diameter. For each droplet size, the number of viruses contained in the droplets can be assumed to follow the Poisson distribution (Anand and Mayya, 2020):

$$P_n = \frac{\mu^n e^{-\mu}}{n!} \tag{1}$$

where P_n is the probability that a droplet of the given size contains n viral copies. The mean expected number of viruses in these droplets, μ, is equal to the product of the droplet volume and the virus concentration (RNA copies mL^{-1}) in the respiratory fluids. It follows that the probability of a droplet of the given size containing at least one virus is $1 - \exp(-\mu)$. For severe COVID-19 cases with a high viral load of 10^8 RNA copies mL^{-1}, theoretical calculations show that the percentage of droplets carrying viruses is 34.3% for droplets 20 μm in diameter prior to evaporative water loss, but only 0.042% for 2-μm droplets. For smaller droplets, even smaller percentages of droplets carry viruses (Anand and Mayya, 2020).

In addition to the number of virions contained in a droplet, the infectivity of viruses in a droplet plays a vital role in airborne transmission. When water evaporates, the salt and protein concentrations in the droplet change, which in turn affect viral infectivity. Several experimental studies on the infectivity of viruses in droplets have been reported with conflicting results.

Drossinos *et al.* (2022) commented in a recent review that, although existing studies were not conclusive regarding the dependence of viral infectivity on ambient relative humidity, the researchers all shared the belief that better understanding of the physical-chemical processes in the droplet was essential for successful resolution of the viral infectivity question.

2.5 Droplet Deposition in the Respiratory Tract

As mentioned earlier, the respiratory tract also acts as a droplet and virion collector. The airway geometry and the aerodynamic characteristics differ among the three regions of the respiratory tract. In consequence, the droplet deposition rate also differs from region to region.

The simple representation of a bronchial airway in Fig. 2 illustrates the mechanisms by which inhaled droplets deposit in the respiratory tract (Wang, 2005). Trajectory 1 shows how a droplet deviates from the airflow streamline and hits the airway wall because of its inertia. Deposition by this mechanism occurs when the airflow changes its direction sharply at a bifurcation. The straight trajectory 2 depicts a droplet falling to the wall by gravity. The irregular trajectory 3 shows how a droplet hits the wall by Brownian motion. A droplet that comes close to the wall, represented by trajectory 4, hits the wall because of its finite size even though it follows the streamline. This deposition mechanism is termed interception. Trajectory 5 illustrates how a charged droplet is attracted to the wall by electrostatic forces. Inertial impaction and gravitational settling are the predominant mechanisms for deposition of larger droplets, while smaller droplets deposit mainly by Brownian diffusion.

When droplets are breathed in, inhaled air blends into humid air in the respiratory tract, which has a relative humidity of approximately 99.5%. The inhaled droplets, which are aqueous solutions containing more than 5% solutes, begin to grow in humid air as a result of water vapor condensation. The increase in droplet size enhances deposition by inertial impaction and gravitational settling in small airways but reduces deposition by Brownian diffusion. The major effects of droplet growth on deposition take place in the bronchioles and the alveolar region.

The fraction of number or mass of inhaled droplets deposited in a respiratory region in a breath is termed deposition fraction. The term refers to the concentration of droplets in the aerosol that

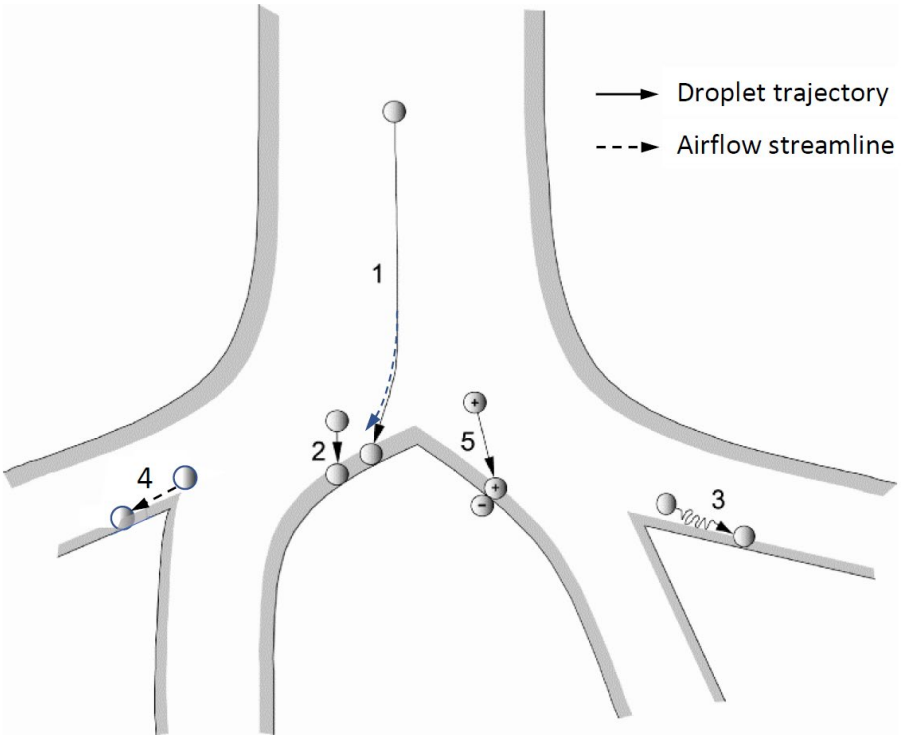

Fig. 2. Mechanisms of particle deposition in the human respiratory tract: 1. inertial impaction, 2. gravitational settling, 3. Brownian motion, 4. interception, 5. electrostatic forces. Adapted from Wang (2005).

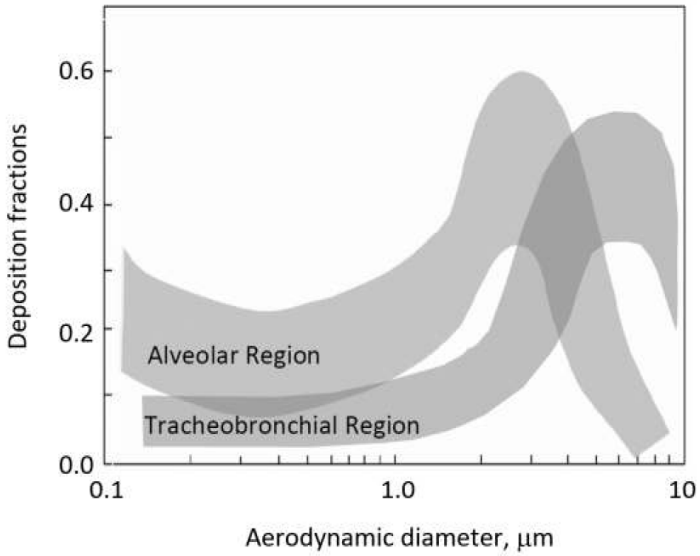

Fig. 3. Deposition fractions in the tracheobronchial and alveolar regions for mouth breathing. Geometric diameter is used for particles smaller than 0.5 μm. Adapted from Wang (2005).

has entered the nose or mouth. Droplet properties, airway dimensions, and breathing patterns are the major factors influencing respiratory deposition. Parameters related to breathing patterns include breathing frequency, tidal volume, the nose and mouth breathing ratio, and the length of pause between inhalation and exhalation. Deposition fractions vary from person to person because each individual has his or her unique airway dimensions and breathing patterns. As a consequence, the deposited viral load differs among individuals exposed to the same concentration of virus-laden droplets.

The two curved bands in Fig. 3, adapted from Wang (2005), show the fractions of inhaled particles deposited in the tracheobronchial and alveolar regions for mouth breathing, respectively. Because of significant person-to-person variation, deposition data from seven experimental studies reported in the literature are plotted as bands. Each band covers all the data on deposition fraction in a respiratory region obtained in the seven experimental studies and can be considered as a collection of the deposition curves of all the volunteers in the experiments. Particles about 6 to 7 μm in aerodynamic diameter have the highest deposition fraction in the tracheobronchial region, and particles about 2 to 3 μm in aerodynamic diameter have the highest deposition fraction in the alveolar region. The aerodynamic diameter and geometric diameter are almost identical for respiratory droplets, which have a density of approximately 1,000 kg m^{-3}.

When droplets are inhaled, larger droplets mainly deposit in the upper airways and the tracheobronchial region, and smaller droplets mainly deposit in the alveolar region. Severe symptoms, such as low oxygen levels, occur when virus-laden droplets are deposited in the tracheobronchial and alveolar regions. Infections in the upper airways are less severe but can spread to the lower two regions.

3 FACE MASKS

The term community transmission refers to the spreading of an infectious disease in a community. A SARS-CoV-2 patient is considered infectious starting two days before symptoms appear or two days before the positive test date if the patient has no symptoms. Transmission from asymptomatic and pre-symptomatic cases makes up at least 50% of community transmission.

Wearing a face mask is an effective non-pharmaceutical intervention measure to reduce respiratory virus transmission. Worn as a source control device, face masks can reduce the chance of infected individuals, who have no symptoms, unknowingly spreading the virus. Face masks can also provide personal protection for the wearers from inhaling virus-laden droplets, which have been transported to their breathing zones.

REVIEW
https://doi.org/10.4209/aaqr.220343

Many types of face masks have been employed in the effort to prevent the spread of respiratory viruses. The most common types include cloth masks, disposable masks, surgical masks (also known as medical procedure masks), and N95 filtering facepiece respirators. Cloth masks and disposable masks give reasonable protection for the general public. For healthcare personnel and people at increased risk for severe disease, surgical masks and N95 respirators can provide higher levels of protection.

The materials used to make face masks include woven and non-woven fabrics. The commonly used melt blown non-woven fabrics are sheets of randomly oriented fibers produced by extruding melted polymer through an orifice die to form filaments and drawing the filaments with hot air flows. The fibers thus produced are about 1 to 5 μm in diameter. Most N95 respirators are made of melt blown fibers.

3.1 Face Mask Efficiency

As a simple and economical device, fibrous filters offer a wide variety of applications, including industrial gas cleaning equipment, indoor air purifiers, and face masks. The basic principles of fibrous filters are well understood. The mechanisms by which a fiber in a fibrous filter captures particles are similar to the mechanisms by which particles deposit in the respiratory tract. They include Brownian motion, inertial impaction, gravitational settling, interception, and electrostatic forces.

The collection efficiency of a fibrous filter depends on particle size, face velocity, and the filter properties. The face velocity is the velocity of air just before it enters the filter. The fibrous filter properties include fiber diameter, filter thickness, fiber charge density, and the volume fraction of fibers in the filter (termed packing density). The penetration, *P*, is the fraction of entering particles that pass through the filter, and the filter efficiency, *E*, is the fraction of entering particles collected by the filter.

The classical theory of fibrous filtration makes use of the concept of single-fiber efficiency. The collection efficiency of a single fiber is defined as the ratio of the number of particles captured by a unit length of a single fiber in the filter to the number of particles in the unperturbed upstream moving through the projected area of the fiber section under consideration. The following expression for filter efficiency is derived by making a mass balance for particles in an infinitesimal layer of the filter and then integrating over the entire thickness of the filter (Wang and Otani, 2013):

$$E = 1 - \exp\left[\frac{-4\alpha\eta t}{\pi d_f (1-\alpha)}\right] \tag{2}$$

In the above equation, α is the filter packing density, η the total single-fiber efficiency, t the filter thickness, and d_f the fiber diameter. The total single-fiber efficiency accounts for the collection of particles by all mechanisms. Inertial impaction, gravitational settling, and interception predominate for the collection of larger particles, while Brownian motion is the dominant collection mechanism for submicron particles. For a given filter, the collection efficiency therefore has a U-shaped dependence on the particle size, with the minimum efficiency falling in the particle size range of 0.05–0.5 μm (Hinds, 1999).

3.2 Resistance to Airflow

To make a face mask more comfortable, the resistance to airflow through the mask should be relatively low. The pressure drop across a mask, an indicator of breathability, represents the resistance to airflow. As the sum of drag force of all the fibers in a mask, the pressure drop is directly proportional to the face velocity and the mask thickness, and inversely proportional to the square of the fiber diameter. The pressure drop increases approximately with the mask packing density to the 1.5th power ($a^{1.5}$).

The National Personal Protective Technology Laboratory (NPPTL), a division of the U.S. National Institute for Occupational Safety and Health (NIOSH), is in charge of testing and approving respirators used in U.S. occupational settings. For a NIOSH-approved N95 respirator, the maximum allowable resistance is 35 mm water (343 Pa) at a flow rate of 85 ± 2 L min^{-1} during inhalation, as specified

in 42 CFR (Code of Federal Regulations) Part 84, Subpart K. The corresponding face velocity is 9.3 cm s^{-1} for a breathing flow rate of 85 L min^{-1} and a respirator surface area of 150 cm^2.

3.3 Measurements of Face Mask Efficiency

The collection efficiency of face masks can be measured using respiratory viruses, ambient aerosol particles, or laboratory-generated non-biological aerosols.

Ueki *et al.* (2020) used SARS-CoV-2 virions to investigate the collection efficiencies of cloth masks, surgical masks, and N95 respirators in a biosafety level 3 facility. Two manikin headforms and a droplet collection unit were placed in a test chamber. Virus laden droplets generated by a nebulizer were exhaled continuously through a manikin headform to simulate a mild cough flow at 2 m s^{-1} for 20 minutes. A second headform connected to an artificial ventilator was employed to simulate tidal breathing (tidal volume of 500 mL, respiratory rate of 18 breaths min^{-1}, and gas exchange rate of 50%). Tests were carried out for three different distances (25, 50, and 100 cm) between the two manikin headforms. The nebulizer was charged with 6 ml of virus suspension (5×10^5 plaque forming units). The mass median diameter of the virus-laden droplets just emitted from the nebulizer was 5.5 μm (< 3 μm 20%, 3–5 μm 40%, > 5–8 μm 40%). A gelatin membrane filter collected all the droplets that passed through the second manikin headform. The viral RNA copy number was measured using quantitative real-time reverse transcription PCR, and the quantity of virus determined using the plaque assay.

The total viral RNA copy number in the droplets that passed through the second headform when both headforms were unmasked was used as the control to calculate the penetration for each of the three types of masks tested. When the first headform (the spreader) was covered by a mask and the un-masked headform (the receiver) was placed 50 cm downstream, the viral RNA data showed that the penetration was 0.43, 0.42, 0.04, and 0.003 respectively for cloth masks, surgical masks, N95 respirators, and N95 respirators taped to improve mask fit. The penetration was 0.63, 0.50, 0.14, and 0.10 respectively for the masks tested when the receiver was covered by a mask and the spreader unmasked. These results clearly showed that the N95 respirator had the lowest penetration even when it was attached to the headform without tape. The penetrations were lower for all three types of masks when they were attached to the spreader. The efficiency of a mask is higher for source control than for personal protection, mainly because the droplets are larger when they are just emitted.

Drewnick *et al.* (2021) employed ambient aerosol particles to measure the collection efficiencies and pressure drops for 44 samples of household materials, including 12 pure cotton fabrics, five fabrics containing cotton mixed with synthetics, 11 synthetic fiber samples, eight synthetic household materials, four paper-like materials, and four natural fiber materials. For comparison, three medical masks and one FFP2 respirator (European standard similar to N95) were also tested. For large aerosol particles (0.5–10 μm in diameter), the collection efficiency averaged over all particle sizes was between 20% and 80% for most household materials at low face velocity (5.3 cm s^{-1}). The pressure drops for household materials ranged between 20 and 50 Pa at a face velocity of 5.3 cm s^{-1}.

The study by Drewnick *et al.* (2021) further showed that, by stacking several layers of household materials, an adequate collection efficiency was achieved for homemade face masks with an acceptable pressure drop. It was also found that, when several layers of household materials were stacked together, each layer could be treated as an individual mask and the overall penetration of the whole stack could be estimated by multiplying the penetration values of individual layers.

3.4 Fit Factor

If a face mask is not well fitted to the contours of the face, some air and droplets will move through the gap between the face and the mask. Relative to a perfectly fitted mask, additional droplets will be inhaled if a mask with air leak is used for personal protection, and additional droplets will be emitted if used for source control. The extent of leak can be accessed using quantitative fit testing procedures and expressed by the fit factor, FF, which is defined as the ratio of the droplet concentration outside the mask to the concentration inside. To account for air leak, the fitted filtration efficiency (FFE) of a face mask is calculated as $100 \times (1 - 1/FF)$.

Lindsley *et al.* (2021) measured fit factors with human subjects for different types of face masks

using the PortaCount® N95 Companion protocol, which counts negatively charged particles 40 to 70 nm in diameter. The measured mean fit factor was 164 for a 3M N95 respirator, 79 for a 3M surgical mask, and 1.4 to 4 for reusable cloth face masks.

Skaria and Smaldone (2014) used a manikin headform to measure the pressure drop across several types of face masks. The headform was ventilated via a Harvard pump simulating tidal breathing (tidal volume of 500 mL, respiratory rate of 15 breaths min^{-1}, and duty cycle of 0.5). Tape was employed to seal the mask to the headform face to eliminate leaks. The results showed that the mean pressure drops across the unsealed and sealed N95 respirator were 2.664 and 2.818 mm water (26.11 and 27.62 Pa), respectively. The similarity in pressure drop between unsealed and sealed N95 respirators indicates good fit without sealing. The mean pressure drops were 0.0104 and 0.8166 mm water (0.102 and 8.003 Pa), respectively, for unsealed earloop and fitted surgical masks, and 1.865 and 1.791 mm water (18.28 and 17.55 Pa), respectively, for sealed earloop and fitted surgical masks. For both earloop and fitted surgical masks, the significant difference in pressure drop between unsealed and sealed masks was a clear sign of considerable air leakage around the unsealed mask.

The Centers for Disease Control and Prevention (CDC) tested the following two ways of improving the fit of medical procedure masks: (1) wearing a cloth mask over a medical procedure mask and (2) knotting the ear loops of a medical procedure mask and then tucking in and flattening the extra material close to the face. Each modification substantially improved source control and reduced wearer exposure (Brooks *et al.*, 2021).

The outer seal of a reusable cloth face mask can be significantly improved using a soft, flexible, and adjustable mask fitter. The University of Wisconsin-Madison College of Engineering has provided the design and specifications of such a mask fitter (UW Marketplace, 2020).

It is challenging for men with beards to find well-fitted face masks. Prince *et al.* (2021) used the U.S. Occupational Safety and Health Administration Quantitative Fit Testing Protocol to examine the fitted filtration efficiency of several types of face masks as a function of beard length. The results showed that, among all the face masks tested, N95 respirators had the highest FFE for beard lengths up to 10 mm. The FFE of N95 respirators decreased linearly with beard length, remaining at or above 95% with a beard length of 2.5 mm.

3.5 Face Mask Quality Factor

Different types of face masks give different collection efficiencies with different pressure drops. The mask quality factor, q_m, is useful for comparing diverse types of face masks:

$$q_m = \frac{-\ln P}{\Delta p} \tag{3}$$

where P is the penetration and Δp the pressure drop across the mask. A mask with a low penetration and a low pressure drop has a high quality factor value.

The quality factor is also known as the figure of merit. To compare the quality factor of different face masks, the same face velocity and droplet size should be used to measure or calculate the penetration and the pressure drop.

The values of quality factor for household materials measured by Drewnick *et al.* (2021) ranged between 0.005 and 0.6 Pa^{-1} at a face velocity of 5.3 cm s^{-1}. For comparison, the quality factor of an FFP2 respirator was approximately 0.08 Pa^{-1}. The measurements were made with ambient aerosol particles, 0.5 to10 μm in diameter, and the quality factor values were averaged over all particle sizes.

4 EFFECTIVENESS AND IMPROVEMENTS OF FACE MASKS

4.1 Effectiveness of Face Masks

Correlational studies and modeling have been employed to investigate the effectiveness of face masks. In a study made by Budzyn *et al.* (2021), the data collected for 520 U.S. counties between 1 July and 4 September 2021 were used to calculate the average increase in daily

number of COVID-19 cases per 100,000 children and adolescents aged under 18. Comparison of the data for the week before the start of school and the second week after the start of school showed that the average increase in daily number of cases for the 198 counties with school mask requirements was 16.32 cases, which were 18.53 cases lower than for the 322 counties without school mask requirements.

Stutt *et al.* (2020) employed two modeling approaches to analyze the effectiveness of face masks in reducing the transmission of SARS-CoV-2. The results indicate that the epidemic spread can be mitigated when face masks are worn by the public all the time (even if there are no symptoms). If all individuals are required to wear a mask all the time during lock-down periods, it is possible to suppress the COVID-19 pandemic spread even if the face mask efficiency is only 50% in capturing exhaled droplets.

Howard *et al.* (2021) reviewed the literature and summarized the evidence that demonstrates the effectiveness of extensive face mask use as source control in reducing community transmission of COVID-19. The available evidence suggests that near-universal use of nonmedical masks in combination with practice of complementary public health measures could successfully reduce community spread.

4.2 Improvement of Face Masks

The factors to consider when selecting a face mask include collection efficiency, fit factor, breathability, quality factor, and reusability. Collection efficiency and fit factor should be the first features to consider. Breathability is important if the mask is to be worn for long periods. The quality factor can be considered if the airflow resistance of the mask is acceptable. Reusable masks can help reduce the enormous problem of plastic waste caused by disposable masks.

Electrostatic forces have been employed to enhance the efficiency of fibrous filters (Wang, 2001). For cloth face masks, application of electrostatic forces can be achieved using two or three layers of different fabrics to generate static charges. In the study by Drewnick *et al.* (2021) cited earlier, synthetic materials were found to show an electrostatic contribution at least as significant as deposition by Brownian diffusion for capture of particles up to 100 nm in diameter.

Commercially available electret masks are made of dielectric fibers, which have a quasi-permanent electrical charge. In both multi-layered cloth masks and electret masks, charged fibers polarize neutral droplets and capture them by dielectrophoretic forces. In the presence of electrostatic forces, a fibrous mask can achieve an adequate efficiency at lower packing density and lower pressure drop.

Huang *et al.* (2013) made theoretical calculations to compare the quality factor between a face mask with no static charges and an electret mask that has a charge density of 4×10^{-5} C m^{-2}. The two masks have the same fiber diameter (4 μm), packing density (0.08), and mask thickness (0.2 mm). The calculations were made for the particle diameter range of 0.02 to 5 μm and the face velocity range of 0.5 to 30 cm s^{-1}. Because the charges on mask fibers increase the particle collection efficiency but do not change the resistance to airflow, the quality factor of the electret mask is significantly higher for all particle diameters and face velocities. As an example, the values of quality factor for 1 μm particles at a face velocity of 6 cm s^{-1} are 0.18 and 0.035 Pa^{-1}, respectively, for the electret mask and the mask with no static charges.

Another method of improving mask efficiency is to use nanofibers as the filter media. Face masks made with finer fibers give higher particle collection efficiencies, but also cause higher pressure drops across the mask. It is therefore necessary to consider the quality factor instead of the collection efficiency alone. Theoretical calculations indicate that the filter quality increases with decreasing fiber diameter for particles larger than 0.2 μm in diameter (Hinds, 1999). Wang *et al.* (2008) investigated the filter quality for filters with a single nanofiber layer on a micrometer fiber substrate. Their measurements showed that nanofiber filters had higher filter quality for particles larger than about 0.1 μm in diameter compared to micrometer fiber filters.

In April 2021, the U.S. Biomedical Advanced Research and Development Authority (BARDA) presented the Mask Innovation Challenge: Building Tomorrow's Mask. The competition has the goal of improving comfort, utility, and protective capabilities of face masks. In Phase 1 of the competition, ten winners were selected for improvements in collection efficiency, fit factor, breathability, mask weight, and reusability (BARDA, 2022).

5 CONCLUDING REMARKS

Both face masks and vaccines are useful for reducing respiratory viral infections. Developed for a specific virus, a vaccine is effective at preventing infection from that virus and, in some cases, related viruses, which can be transmitted via various routes, including airborne transmission and fomite transmission. Face masks can help reduce airborne transmission of all types of respiratory viruses. They are the best defense before vaccines are developed for a new virus. Together with ventilation, face masks can significantly reduce the probability of transmission in indoor settings. While face masks have proven adequate in reducing airborne transmission of SARS-CoV-2 infections, there is room for improvement.

According to the World Health Organization Coronavirus (COVID-19) Dashboard (WHO, 2022), more than 600 million confirmed cases of COVID-19 have been reported globally as of 6 September 2022. The diameter, volume, and mass of a SARS-CoV-2 virus are approximately 100 nm, 10^{-15} cm^3, and 10^{-15} g, respectively. An infected individual during peak infection carries 10^9 to 10^{11} virions (Sender *et al.*, 2021). Accordingly, all virions carried by 600 million human hosts during peak infection just have a mass of 0.6 to 60 kg. It is hard to believe that no more than 60 kg of the SARS-CoV-2 virions can infect 600 million people. There is no doubt that new and more infectious types of respiratory viruses will emerge in the years to come. Continuing effort to improve face masks is a proactive measure to prepare for the future respiratory viral threats.

ACKNOWLEDGEMENTS

The author thanks Susan L. Wang for helpful suggestions.

CONFLICT OF INTEREST

The author declares no conflict of interest.

REFERENCES

Anand, S., Mayya, Y.S. (2020). Size distribution of virus laden droplets from expiratory ejecta of infected subjects. Sci. Rep. 10, 21174. https://doi.org/10.1038/s41598-020-78110-x

Asadi, S., Anthony S, W., Cappa, C.D., Barreda, S., Bouvier, N.M., Ristenpart, W.D. (2019). Aerosol emission and superemission during human speech increase with voice loudness. Sci. Rep. 9, 2348. https://doi.org/10.1038/s41598-019-38808-z

BARDA (2022). Mask Innovation Challenge. https://www.drive.hhs.gov/mask_challenge.html (accessed 2 May 2022)

Brooks, J.T., Beezhold, D.H., Noti, J.D., Coyle, J.P., Derk, R.C., Blachere, F.M., William G. Lindsley (2021). Maximizing fit for cloth and medical procedure masks to improve performance and reduce SARS-CoV-2 transmission and exposure. Morb. Mortal. Wkly. Rep. 70, 254–259. https://doi.org/10.15585/mmwr.mm7007e1

Budzyn, S.E., Panaggio, M.J., Parks, S.E., Papazian, M., Magid, J., Barrios, L.C. (2021). Pediatric COVID-19 cases in counties with and without school mask requirements -- United States, July 1-September 4, 2021. Morb. Mortal. Wkly. Rep. 70, 1377–1378. https://doi.org/10.15585/mmwr.mm7039e3

Drewnick, F., Pikmann, J., Fachinger, F., Moormann, L., Sprang, F., Borrmann, S. (2021). Aerosol filtration efficiency of household materials for homemade face masks: Influence of material properties, particle size, particle electrical charge, face velocity, and leaks. Aerosol Sci. Technol. 55, 63–79. https://doi.org/10.1080/02786826.2020.1817846

Drossinos, Y., Reid, J.P., Hugentobler, W., Stilianakis, N.I. (2022). Challenges of integrating aerosol dynamics into SARS-CoV-2 transmission models. Aerosol Sci. Technol. 56, 777–784. https://doi.org/10.1080/02786826.2022.2102792

Effros, R.M., Hoagland, K.W., Bosbous, M., Castillo, D., Foss, B., Dunning, M., Gare, M., Lin, W., Sun, F. (2002). Dilution of respiratory solutes in exhaled condensates. Am. J. Respir. Crit. Care

Med. 165, 663–669. https://doi.org/10.1098/rsif.2017.0939
Hinds, W.C. (1999). Aerosol Technology: Properties, Behavior, and Measurement of Airborne Particles, Second Edition. John Wiley & Sons, Inc., New York.
Howard, J., Huang, A., Li, Z., Tufekci, Z., Zdimal, V., van der Westhuizen, H.M., von Delft, A., Price, A., Fridman, L., Tang, L.H., Tang, V., Watson, G.L., Bax, C.E., Shaikh, R., Questier, F., Hernandez, D., Chu, L.F., Ramirez, C.M., Rimoin, A.W. (2021). An evidence review of face masks against COVID-19. Proc. Natl. Acad. Sci. U.S.A. 118, e2014564118. https://doi.org/10.1073/pnas.2014564118
Huang, S.H., Chen, C.W., Kuo, Y.M., Lai, C.Y., McKay, R., Chen, C.C. (2013). Factors affecting filter penetration and quality factor of particulate respirators. Aerosol Air Qual. Res. 13, 162–171. https://doi.org/10.4209/aaqr.2012.07.0179
Johnson, G.R., Morawska, L., Ristovski, Z.D., Hargreaves, M., Mengersen, K., Chao, C.Y.H., Wan, M.P., Li, Y., Xie, X., Katoshevski, D., Corbett, S. (2011). Modality of human expired aerosol size distributions. J. Aerosol Sci. 42, 839–851. https://doi.org/10.1016/j.jaerosci.2011.07.009
Lindsley, W.G., Blachere, F.M., Beezhold, D.H., Law, B.F., Derk, R.C., Hettick, J.M., Woodfork, K., Goldsmith, W.T., Harris, J.R., Duling, M.G., Boutin, B., Nurkiewicz, T., Boots, T., Coyle, J., Noti, J.D. (2021). A comparison of performance metrics for cloth masks as source control devices for simulated cough and exhalation aerosols. Aerosol Sci. Technol. 55, 1125–1142. https://doi.org/10.1080/02786826.2021.1933377
Morawska, L., Johnson, G.R., Ristovski, Z.D., Hargreaves, M., Mengersen, K., Corbett, S., Chao, C.Y.H., Li, Y., Katoshevski, D. (2009). Size distribution and sites of origin of droplets expelled from the human respiratory tract during expiratory activities. J. Aerosol Sci. 40, 256–269. https://doi.org/10.1016/j.jaerosci.2008.11.002
Nicas, M., Nazaroff, W.W., Hubbard, A. (2005). Toward understanding the risk of secondary airborne infection: Emissions of respirable pathogens. J. Occup. Environ. Hyg. 2, 1545–9632. https://doi.org/10.1080/15459620590918466
Prince, S.E., Chen, H., Tong, H., Berntsen, J., Masood, S., Zeman, K.L., Clapp, P.W., Bennett, W.D., Samet, J.M. (2021). Assessing the effect of beard hair lengths on face masks used as personal protective equipment during the COVID-19 pandemic. J. Exposure Sci. Environ. Epidemiol. 31, 953–960. https://doi.org/10.1038/s41370-021-00337-1
Sender, R., Bar-on, Y.M., Gleizer, S., Bernshtein, B., Milo, R. (2021). The total number and mass of SARS-CoV-2 virions. PNAS 118, 1–9. https://doi.org/10.1073/pnas.2024815118
Skaria, S.D., Smaldone, G.C. (2014). Respiratory source control using surgical masks with nanofiber media. Ann. Occup. Hyg. 58, 771–781. https://doi.org/10.1093/annhyg/meu023
Stadnytskyi, V., Anfinrud, P., Bax, A. (2021). Breathing, speaking, coughing or sneezing: What drives transmission of SARS-CoV-2? J. Intern. Med. 290, 1010–1027. https://doi.org/10.1111/joim.13335
Stutt, R.O.J.H., Retkute, R., Bradley, M., Gilligan, C.A., Colvin, J. (2020). A modelling framework to assess the likely effectiveness of facemasks in combination with 'lock-down' in managing the COVID-19 pandemic. Proc. R. Soc. London, Ser. A 476, 20200376. https://doi.org/10.1098/rspa.2020.0376
Ueki, H., Furusawa, Y., Iwatsuki-Horimoto, K., Imai, M., Kabata, H., Nishimura, H., Kawaoka, Y. (2020). Effectiveness of face masks in preventing airborne transmission of SARS-CoV-2. mSphere 5, e00637–00620. https://doi.org/10.1128/mSphere.00637-20
UW Marketplace (2020). Badger Seal. https://making.engr.wisc.edu/mask-fitter/ (accessed 2 May 2022)
Wang, C.C., Prather, K.A., Sznitman, J., Jimenez, J.L., Lakdawala, S.S., Tufekci, Z., Marr, L.C. (2021). Airborne transmission of respiratory viruses. Science 373, 981. https://doi.org/10.1126/science.abd9149
Wang, C.S. (2001). Electrostatic forces in fibrous filters: A review. Powder Technol. 118, 166–170. https://doi.org/10.1016/S0032-5910(01)00307-2
Wang, C.S. (2005). Inhaled particles. Elsevier Academic Press, Amsterdam.
Wang, C.S., Otani, Y. (2013). Removal of nanoparticles from gas streams by fibrous filters: A review. Ind. Eng. Chem. Res. 52, 5–17. https://doi.org/10.1021/ie300574m
Wang, J., Kim, S.C., Pui, D.Y.H. (2008). Investigation of the figure of merit for filters with a single nanofiber layer on a substrate. J. Aerosol Sci. 39, 323–334. https://doi.org/10.1016/j.jaerosci.2007.12.003

World Health Organization (WHO) (2022). WHO Coronavirus (COVID-19) Dashboard. https://covid19.who.int/ (accessed 7 September 2022)

Wölfel, R., Corman, V.M., Guggemos, W., Seilmaier, M., Zange, S., Müller, M.A., Niemeyer, D., Jones, T.C., Vollmar, P., Rothe, C., Hoelscher, M., Bleicker, T., Brünink, S., Schneider, J., Ehmann, R., Zwirglmaier, K., Drosten, C., Wendtner, C. (2020). Virological assessment of hospitalized patients with COVID-2019. Nature 581, 465–469. https://doi.org/10.1038/s41586-020-2196-x